Improving slope deformation and stability predictions in anisotropic rock masses: A strain- and confinement-dependent dilation model for ubiquitous joints

Farahmand, K. *Knight Piesold, Vancouver, Canada*

Rahjoo, M. *University of British Columbia, Vancouver, Canada*

Abstract

Open-pit slope stability analyses rely not only on predicting failure but also on reproducing realistic deformation patterns for calibration against field monitoring data. In common numerical practice, uniform and low-value dilation angles are adopted to constrain dilation-induced volumetric expansion and the resulting displacement magnitudes in numerical models. This simplification overlooks the strong dependence of dilation on shear history and confinement stress, frequently leading to displacement fields that are inconsistent with prism and LiDAR measurements used in operational slope monitoring.

This paper presents a strain-softening and confinement-dependent dilation formulation developed specifically for ubiquitous joints in FLAC3D. The mobilized dilation angle is defined as a function of accumulated plastic shear strain and effective normal stress, allowing dilation to degrade progressively with shear and to be suppressed under increasing confinement. Comparative numerical examples demonstrate that the proposed formulation produces more realistic displacement gradients, localized deformation, and shallower failure mechanisms relative to constant-dilation assumptions. These improvements enhance the ability to calibrate numerical models against monitored slope movements, supporting observational and performance-based design approaches for the management of critically deforming pit walls.

1. Introduction

Accurate prediction of open-pit slope performance requires realistic modelling of rock mass deformation, not merely assessment of stability at failure. In practice, slope behaviour is continuously monitored using prism networks installed along the crest, mid-slope, and toe, together with LiDAR and radar systems that provide spatially continuous measurements of displacement magnitude and deformation trends. These monitoring datasets form the primary basis for calibrating numerical models, validating geomechanical assumptions, and managing slope risk through observational design.

Despite this, many numerical slope models represent dilation using a uniform, constant angle—typically in the range of 0° to 5°—applied to all yielding material for both rock matrix and structures such as joints (Farahmand and Rahjoo, 2025). While this simplification is often adopted to limit excessive deformation predictions, it introduces important limitations. Constant-dilation models neglect the strong dependence of dilatancy on shear history and confinement, frequently producing displacement patterns that are inconsistent with monitored behaviour. In particular, such models tend to over-restrict deformation at depth while exaggerating bulking near failure surfaces, forcing practitioners to compensate through unrealistic adjustment of stiffness or strength parameters during calibration.

Laboratory and field evidence demonstrate that rough rock joints can mobilize substantial dilation at the onset of shearing under low normal stress, with dilation angles commonly in the range of 10°–20° (e.g. Ladanyi & Archambault 1969; Goodman 1976; Barton et al. 1985). During shearing of non-planar joints, surface asperities slide and override one another, producing displacement normal to the joint plane (i.e. dilation) as joint aperture increases (Barton et al. 1985). As shear displacement accumulates, dilation capacity degrades rapidly due to asperity damage, and under high confinement dilation is strongly suppressed or eliminated altogether. These mechanisms are critical for reproducing the gradual displacement gradients and curvature of deformation fields commonly observed in prism and LiDAR monitoring data, and form the physical basis illustrated

in Figure 1. As a result, numerical models may underestimate deformation during the early stages of failure—when dilation is most pronounced—while simultaneously overestimating dilation at depth, where confinement is high, and failing to account for enhanced dilation near low-constraint regions such as convex slope faces.

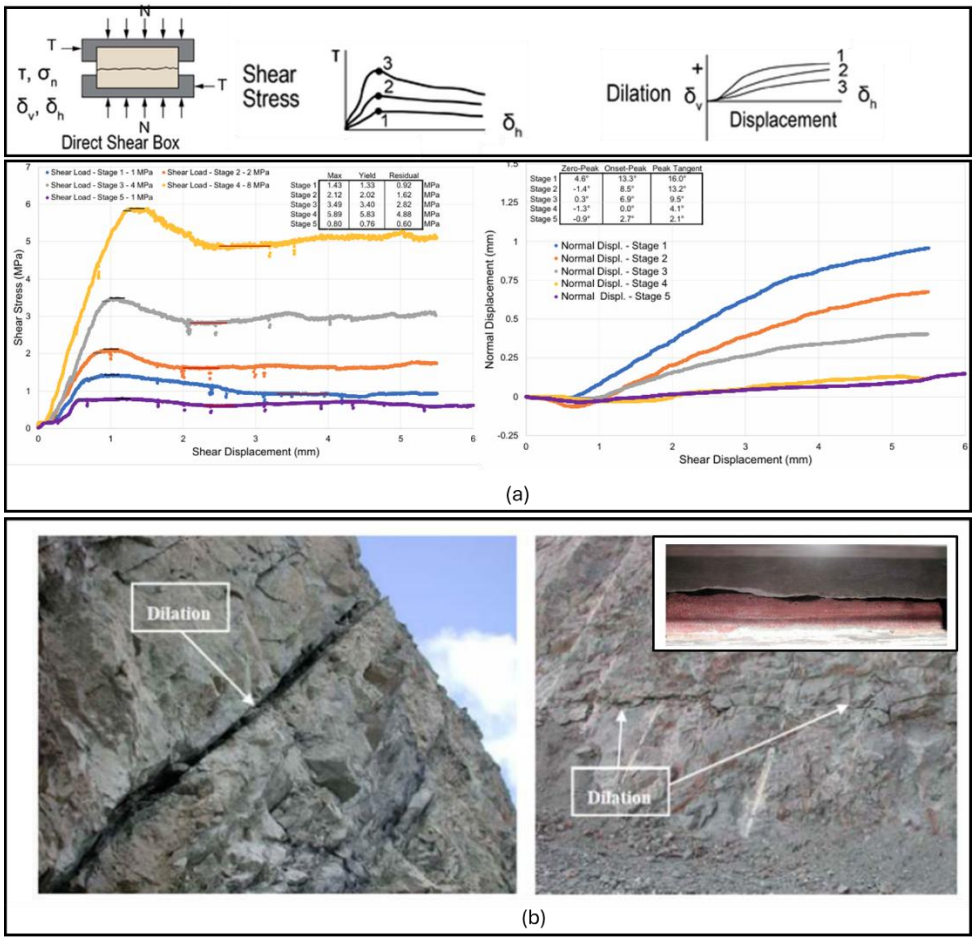


Figure 1. Physical basis of joint dilation. (a) Conceptual shear-induced dilation from direct shear testing of unfilled rock fractures (MacDonald et al., 2023). (b–c) Field examples of dilative joint behaviour in rock slopes (Sullivan, 2007; Farahmand et al., 2015).

Recent work by Rahjoo and Eberhardt (2021) and Farahmand and Rahjoo (2025) demonstrated that strain- and confinement-dependent dilation formulations substantially improve the realism of predicted deformation and failure geometry in slope analyses. These studies showed that accounting for post-peak dilation degradation leads to shallower, more localized failure mechanisms and displacement patterns that better reflect observed slope behaviour. However, these formulations were developed primarily for intact rock behaviour using PSIR-based approaches.

In many open-pit slopes, deformation and failure are governed by one or more dominant joint or bedding sets, making it both practical and necessary to apply advanced dilation modelling directly to structural discontinuities. Building on prior work, the present study develops a strain-softening and confinement-dependent dilation model tailored specifically to the ubiquitous joint formulation in FLAC3D. By embedding physically realistic dilation behaviour within a standard continuum framework commonly used in industry, the proposed approach improves the ability of numerical models to reproduce observed deformation patterns, facilitates more defensible calibration against monitoring data, and supports performance-based and observational slope design for the management of critically deforming pit walls.

2. Theoretical formulation of the ubiquitous joint dilation model

When a rock joint, or any discrete shear surface, undergoes shearing, dilation commonly occurs as a result of asperity interlocking. This process causes the opposing joint surfaces to separate normal to the shear plane, producing a net volumetric expansion. The dilation angle, ψ_j, is defined as the ratio of incremental normal displacement to incremental shear displacement along the joint:

$$\psi_j = arctan\left(\frac{\Delta V}{\Delta H}\right) \quad [1]$$

where ΔV represents the incremental normal (volumetric) expansion and ΔH denotes the incremental shear displacement. For a given joint, the dilation angle is not a fixed material property. Instead, it evolves as a function of shear history and the effective normal stress acting on the joint surface. At small shear displacements, rough joints can mobilize relatively large dilation angles, in some cases exceeding 20° for fresh, highly interlocked surfaces subjected to low normal stress. As shearing progresses, however, asperity damage and smoothing lead to a gradual reduction in dilation, ultimately approaching a residual state characterized by negligible volumetric expansion.

Normal stress exerts a similarly strong influence on joint dilation. Under low confinement, joint surfaces are free to lift and rotate during shear, allowing dilation to develop. With increasing normal stress—such as at depth within a slope or under substantial external confinement—the ability of asperities to dilate is progressively restricted. In such conditions, shearing tends to occur with limited or no dilation as asperities are either overridden or crushed.

These trends are well established in experimental studies of joint behaviour. Direct shear tests, for example, commonly show dilation angles on the order of 10°–20° at normal stresses around 0.1 MPa, while the same joints tested under normal stresses of 1–2 MPa may mobilize dilation angles of only a few degrees or less. This stress- and roughness-dependent behaviour forms the basis of widely used empirical descriptions, including the Barton and Choubey (1977) JRC–JCS criterion for rock joints, as well as later rock-mass-scale formulations proposed by Zhao and Cai (2010) and Walton and Diederichs (2015).

3. Proposed formulation of the ubiquitous joint dilation model

To represent the combined influence of shear history and confinement on joint dilation, the mobilized dilation angle of the ubiquitous joint, ψ_j, is expressed as a peak value scaled by independent strain- and stress-dependent reduction factors

$$tan\,\psi_j(\gamma^{pl,j}, \sigma_{n,j}) = tan\,\psi_{0,j} \cdot F_\gamma(\gamma^{pl,j}) \cdot F_{\sigma_n}(\sigma_{n,j}) \quad [2]$$

where γ_j^{pl} is the accumulated plastic shear strain associated with slip on the joint plane and $\sigma_{n,j}$ is the effective normal stress acting on that plane. The parameter $\psi_{0,j}$ denotes the peak dilation angle mobilized at the onset of shearing under very low confinement and reflects joint surface roughness and strength. The functions F_γ and F_{σ_n} independently control the progressive reduction of dilation with shear deformation and increasing confinement, respectively.

3.1 Strain-Softening Mobilization Factor $F_\gamma(\gamma_j^{pl})$

The strain-dependent factor F_γ accounts for the progressive degradation of dilation capacity as shear displacement accumulates. Physically, this represents the breakdown and wear of joint asperities, which leads to a reduction in dilatancy beyond peak conditions. The function satisfies:

$F_\gamma(0) = 1, F_\gamma(\infty) \to 0$ ensuring full mobilization of $\psi_{0,j}$ at the onset of shear and negligible dilation at large strains.

In this study, a smooth exponential decay is adopted:

$$F_\gamma(\gamma_j^{pl}) = exp\left(-\frac{\gamma_j^{pl}}{\gamma_{m,j}}\right) \quad [3]$$

where $\gamma_{m,j}$ is a characteristic plastic shear strain at which the mobilized dilation has reduced to $e^{-1} \approx 0.37$ of its peak value. This formulation captures the commonly observed rapid post-peak reduction of dilation followed by a gradual asymptotic approach toward residual, non-dilative behaviour. The exponential form has been widely used in constitutive modeling of jointed rock masses and provides a compact and numerically stable representation of strain-softening dilatancy.

3.2 Confinement (Normal Stress) Factor $F_{\sigma_n}(\sigma_{n,j})$

The confinement-dependent factor F_{σ_n} represents the suppression of dilation with increasing effective normal stress. Under low confinement, joint surfaces are free to dilate, whereas under higher normal stress asperity interlocking is increasingly constrained, leading to reduced or negligible dilation. The confinement factor satisfies: $F_{\sigma_n}(0) = 1, F_{\sigma_n}(\infty) \to 0$.

An exponential form is adopted:

$$F_{\sigma_n}(\sigma_{n,j}) = exp(-\alpha\, \sigma_{n,j}) \quad [4]$$

where α is a decay constant with units of inverse stress. The effective normal stress acting on the joint plane is assumed non-negative ($\sigma_{n,j} \geq 0$), such that $F_{\sigma_n} = 1$ at zero confinement and decreases monotonically with increasing normal stress.

For convenience and physical interpretability, α is defined in terms of a reference normal stress $\sigma_{n,\text{ref},j}$ at which dilation is reduced by half:

$$\boldsymbol{\alpha = \frac{ln\, 2}{\sigma_{n,ref,j}}} \quad [5]$$

With this definition, $F_{\sigma_n}(\sigma_{n,\text{ref},j}) = 0.5$. The exponential confinement function closely reproduces the logarithmic reduction of dilation with increasing normal stress observed in laboratory direct-shear tests and encapsulated in Barton-type empirical relationships, while remaining straightforward to calibrate and implement.

Taken together, the strain- and stress-dependent reduction functions ensure that the peak dilation angle $\psi_{0,j}$ is mobilized only under conditions where it is mechanically plausible—namely, during early stages of shearing and under low confinement. As either accumulated plastic shear strain increases or normal stress rises, the mobilized dilation angle ψ_j is progressively reduced. The resulting formulation defines a non-associative flow rule in which dilation evolves continuously with the mechanical state of the joint rather than remaining constant throughout deformation.

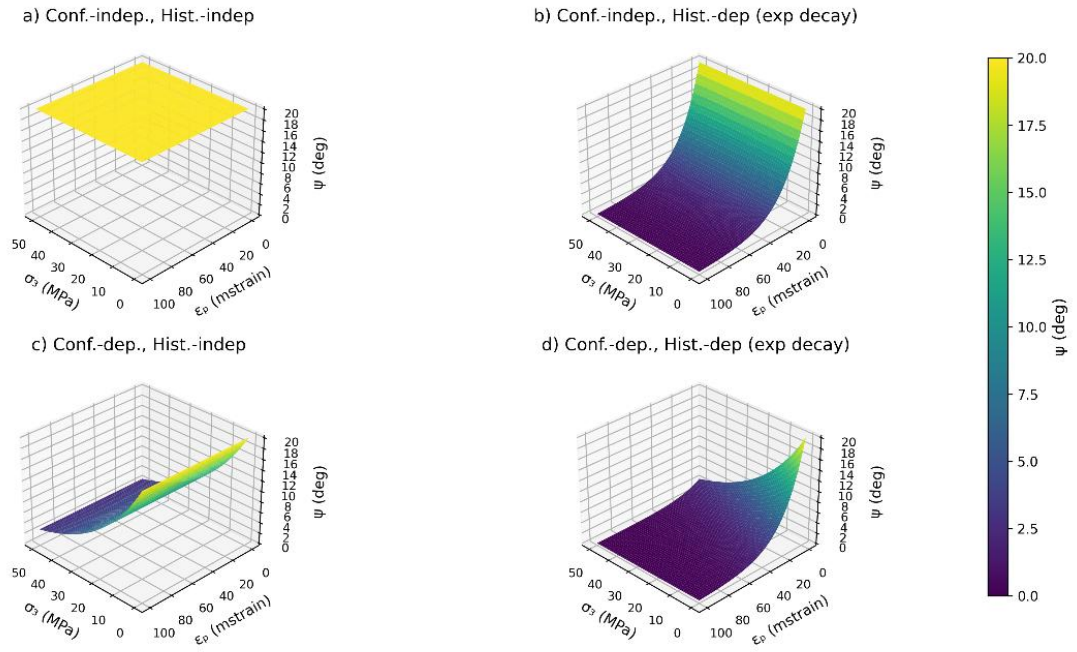


Figure 2. Comparison of mobilized ubiquitous-joint dilation angle ψ_j under different constitutive assumptions: (a) constant dilation; (b) strain-dependent only; (c) confinement-dependent only; and (d) combined strain- and confinement-dependent formulation.

3.3 Optional Intermediate Principal Stress Effect

Because the ubiquitous joint model is inherently planar, the confinement factor F_{σ_n} primarily captures the influence of the minimum principal stress S_3 through the effective normal stress acting on the joint plane. In fully three-dimensional stress states, however, the intermediate principal stress S_2 can further influence dilative behaviour. To account for this effect, an optional scaling factor F_b may be introduced as a function of the stress-state index: $b = \frac{S_2 - S_3}{S_1 - S_3}$

If employed, F_b can be used to further modulate the confinement factor, for example by reducing dilation under stress states approaching triaxial extension. In the present implementation, this factor is treated as a secondary refinement intended for highly anisotropic or strongly curved slope geometries. The core model behaviour and results presented herein are governed predominantly by the strain-dependent factor F_γ and the confinement factor F_{σ_n}.

3.4 Relation to PSIR-Based Dilation Models for the Rock Matrix

Building on the work of Rahjoo (2019), Farahmand and Rahjoo (2025) extended strain- and confinement-dependent dilation concepts to the intact rock matrix using a plastic strain increment ratio (PSIR)–based framework. This formulation explicitly accounts for three-dimensional stress effects, including the influence of the intermediate principal stress S_2, and describes dilation as an evolving response controlled by plastic strain accumulation and confinement.

In the PSIR framework, the mobilized dilation response of the rock matrix is expressed as

$$N_\psi\left(S_3, S_2, \gamma^{pl}\right) = N_{\psi 0}\, F_{\gamma^p}\left(\gamma^{pl}\right) \cdot\ F_{S_3}(S_3)\ \cdot F_b(b) \qquad [6]$$

where N_ψ is the plastic strain increment ratio governing dilatancy, $N_{\psi 0}$ is the peak PSIR mobilized under an asymmetric stress state at $S_3 = 0$, and γ^{pl} is the accumulated plastic shear strain.

The post-peak degradation of dilation with plastic straining is captured through the strain-dependent function

$$F_{\gamma^p}(\gamma^{pl}) = exp\left(-\frac{\gamma^{pl}}{\gamma_m}\right) \quad [7]$$

where γ_m is a material parameter controlling the rate of dilation decay. In slope stability analyses, the magnitude of pre-peak dilation is typically negligible relative to post-peak dilatancy, and the formulation is therefore primarily governed by post-peak plastic strain accumulation.

The suppression of dilation with increasing confinement is described by

$$F_{S_3}(S_3) = \begin{cases} \left(\frac{1}{N_{\psi 0}} - 1\right)\left(\frac{S_3}{S_3^{cv}}\right) + 1, & 0 < S_3 < S_3^{cv} \\ \frac{1}{N_{\psi 0}}, & S_3 \geq S_3^{cv} \end{cases} \quad [8]$$

where S_3^{cv} is the critical confinement beyond which dilation is fully suppressed.

The influence of stress-state anisotropy is incorporated through an intermediate principal stress factor

$$F_b(b) = \begin{cases} \frac{1}{2}\left(\frac{b}{b_1}\right) + \frac{1}{2}, & 0 < b < b_1 \\ 1, & b_1 \leq b < b_2 \\ \left(\frac{b - b_2}{1 - b_2}\right) + 1, & b_2 \leq b \leq 1 \end{cases} \quad [9]$$

with the stress-state index defined as

$$b = \frac{S_2 - S_3}{S_1 - S_3} \quad [10]$$

Here, γ_m, S_3^{cv}, b_1, and b_2 are model parameters controlling strain softening, confinement suppression, and stress-state dependence, respectively. The formulation is intentionally constructed to be S_2-independent under highly asymmetric stress states, consistent with Mohr–Coulomb–based dilation assumptions.

While the PSIR-based model targets dilation of the rock matrix, the present study adapts the same underlying physical principles—namely strain-dependent degradation and confinement-dependent suppression of dilation—to the ubiquitous joint formulation commonly used in slope stability analyses. In contrast to the PSIR framework, dilation in the ubiquitous joint model is expressed through an evolving joint dilation angle rather than a plastic strain increment ratio. Nevertheless, both approaches share a common conceptual basis and predict similar trends in deformation localization and failure geometry when applied under comparable stress conditions.

4. Calibration and literature guidance

Selection of dilation-related parameters for numerical modelling with the ubiquitous joint formulation (e.g. in FLAC3D) was guided by published experimental data and empirical descriptions of joint behaviour, rather than by direct calibration to the slope response. Emphasis was placed on ensuring that the adopted parameters produce dilation magnitudes and confinement sensitivity that are mechanically plausible and consistent with laboratory observations.

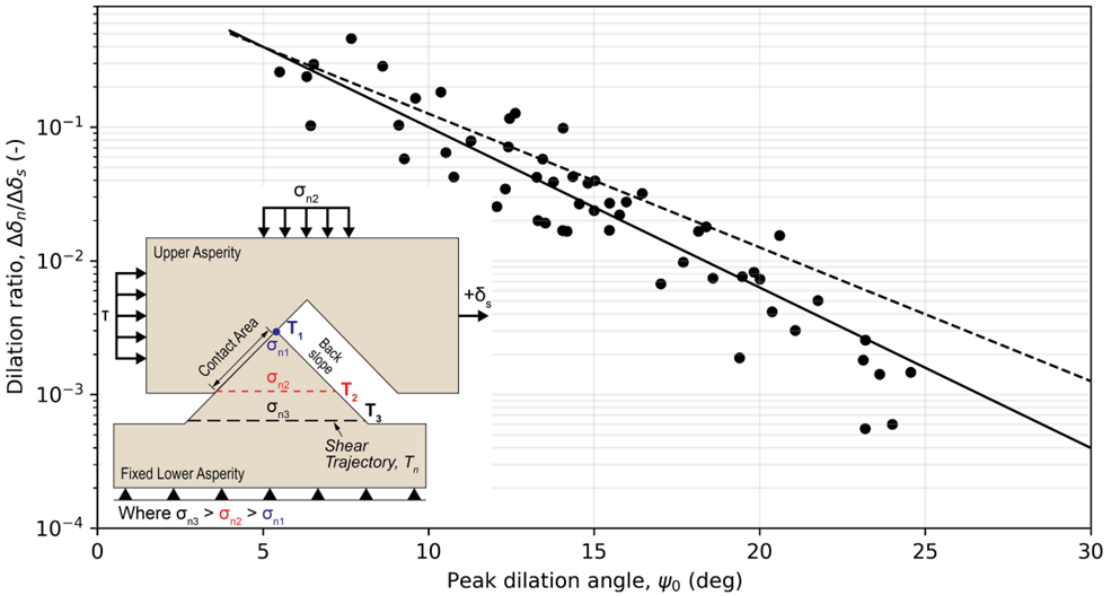


Figure 3. Peak dilation angle response of varying ratios of normal stress to compressive strength (modified after Barton, 1973 and MacDonald et al., 2023).

Figure 3 illustrates the classical dependence of peak joint dilation on effective normal stress, expressed in terms of the ratio of normal stress to joint compressive strength, modified after Barton (1973) and MacDonald et al. (2023). These data demonstrate that dilation can be substantial under low confinement but decreases rapidly with increasing normal stress, particularly for rough, strong joints. Although Barton-type relationships are not implemented directly in the present formulation, they provide an important conceptual reference for bounding both the magnitude of peak dilation and the rate at which dilation is suppressed with confinement. Figure 3 provides conceptual bounds on the magnitude and confinement sensitivity of joint dilation, while Tables 1 and 2 translate these trends into practical parameter ranges governing confinement-dependent and strain-dependent dilation, respectively.

Representative values of residual friction angle ϕ_r were selected based on ISRM Suggested Methods (1978) and subsequent studies. Typical dry values include metamorphic and igneous rocks ($\phi_r \approx 30^\circ \pm 5^\circ$), sedimentary rocks such as sandstones and limestones ($\phi_r \approx 25^\circ$–35°), phyllites and slates ($\phi_r \approx 20^\circ$–30°), and schists ($\phi_r \approx 25^\circ$, potentially lower where foliation surfaces are mica-rich). These values generally correspond to dry conditions and should be reduced by several degrees for saturated joints. Soft rocks or clay-rich joint surfaces may exhibit substantially lower residual friction angles, for example shales and claystones with $\phi_r \approx 10^\circ$–20°.

The confinement sensitivity of dilation is controlled in the proposed model through the reference normal stress $\sigma_{n,\mathrm{ref},j}$, defined as the effective normal stress at which the mobilized dilation angle is reduced to 50 % of its peak value. This parameter reflects joint roughness, surface strength, and infilling characteristics. Practical ranges of $\sigma_{n,\mathrm{ref},j}$, consistent with laboratory observations and field back-analyses, are summarized in Table 1. These ranges translate the qualitative trends illustrated in Figure 3 into parameter values suitable for numerical implementation.

The strain-softening parameter $\gamma_{m,j}$ governs the rate at which dilation degrades with accumulated plastic shear strain along the joint plane. Smaller values correspond to rapid post-peak degradation of dilation associated with brittle asperity damage, whereas larger values imply more gradual decay. Typical ranges, expressed in terms of accumulated plastic shear strain, are summarized in Table 2. Because $\gamma_{m,j}$ is strain-based, its numerical effect is mesh-dependent and should be calibrated consistently with zone size and the expected thickness of the shear band.

Table 1. Suggested reference normal stress ranges for joint dilation suppression.

Joint Condition/ Rock Type	Suggested $\sigma_{n,\mathrm{ref,j}}$ Range (MPa)
Very soft or clay-filled joints	0.1 – 1
Moderately strong rock joints (e.g., shale)	1 – 5
Strong, rough rock joints (e.g., granite)	5 – 15
Very strong, interlocked joints	10 – 20

Table 2. Suggested ranges for dilation strain-softening parameter $\gamma_{m,j}$

Joint Type/ Behaviour	Suggested $\gamma_{m,j}$ Range
Very brittle, low-displacement joints	0.001 – 0.01
Moderately rough joints (typical rock masses)	0.01 – 0.05
Highly rough or gouge-filled joints	0.05 – 0.10+

Where estimates of the Joint Roughness Coefficient (JRC) and Joint Compressive Strength (JCS) are available, Barton's empirical criterion provides useful guidance for bounding peak dilation behaviour. Barton and Choubey (1977) proposed that the peak dilation component—approximately equal to the difference between peak and residual friction angles—may be expressed as

$$\psi_{peak,j} \approx \phi_{peak} - \phi_r \approx JRC log_{10}\left(\frac{JCS}{\sigma_n}\right) \quad [11]$$

This relationship provides insight into the sensitivity of joint dilation to effective normal stress σ_n.

For example, a joint with $\mathrm{JRC} \approx 10$and $\mathrm{JCS} = 100$ MPa would mobilize a dilation component of approximately 30° at $\sigma_n = 0.1$ MPa, reducing to about 20° at $\sigma_n = 1$ MPa. If the former represents the maximum dilation under near-zero confinement, the mobilized dilation at 1 MPa corresponds to roughly two-thirds of the peak value, implying $F_{\sigma_n}(1\,\mathrm{MPa}) \approx 0.67$. A hyperbolic confinement-reduction function reproducing this behaviour would therefore require $\sigma_{n,\mathrm{ref}} \approx 1$ MPa.

For smoother joints (e.g., $\mathrm{JRC} \approx 4$) or joints with lower JCS values, the same level of confinement may suppress dilation by 80–90%, corresponding to significantly smaller values of $\sigma_{n,\mathrm{ref}}$, often on the order of a few hundred kilopascals. In this way, Barton's criterion provides a practical framework for selecting $\sigma_{n,\mathrm{ref}}$ by matching modeled dilation suppression to joint roughness characteristics and the expected stress range.

It is important to emphasize that $\gamma_{m,j}$, being expressed in terms of plastic shear strain rather than displacement, is inherently dependent on zone size. In FLAC3D, plastic shear strain is computed as shear displacement divided by zone dimension ($\gamma_j^{pl} \approx \Delta u_s \,/\, \Delta z$), so a given displacement produces a smaller strain in a larger zone. The characteristic displacement at which dilation degrades to 1/e of its peak is $d_{m,j} = \gamma_{m,j} \times \Delta z$. For example, $\gamma_{m,j} = 0.001$ in a 2 m zone implies $d_{m,j} \approx 2$ mm, consistent with brittle lab joints; in a 10 m zone, the same value implies $d_{m,j} \approx 10$ mm — a different physical response. This mesh dependency is an inherent characteristic of all strain-softening models in continuum frameworks, arising because real joints localize deformation in narrow shear bands (millimetres to centimetres), whereas continuum zones average this over a much larger volume. In practice, $\gamma_{m,j}$ should be selected so that $d_{m,j}$ is consistent with post-peak

dilation degradation observed in direct shear tests, and adjusted proportionally if the mesh is refined or coarsened.

5. Mechanical Implications for Stress and Displacement Fields

In FLAC3D, zone displacements arise from the accumulation of elastic and plastic strain increments associated with all active constitutive mechanisms. When both matrix and ubiquitous joint plasticity are present, volumetric strain contributions from each mechanism are additive. In practice, however, deformation patterns are dominated by the mechanism accumulating the larger plastic shear strain. Consequently, along joint-controlled failure surfaces, degradation of ubiquitous joint dilation primarily governs the displacement and volumetric response, while matrix dilation becomes significant only in regions where matrix yielding is extensive.

5.1 Shear-Induced Volumetric Strain and Displacements

A non-zero dilation angle implies that shear failure is accompanied by volumetric expansion. In numerical simulations employing the ubiquitous joint formulation, this response manifests as localized bulking of zones undergoing shear, whereby the failed material occupies a larger volume than in its pre-failure state. For example, shear bands developing with $\psi_j > 0$ may generate outward or upward displacements near free surfaces, producing localized heave at slope faces or toes.

In more confined settings, such as slope interiors or beneath overburden, the same dilative tendency is constrained by the surrounding rock mass. Under these conditions, volumetric expansion is accommodated primarily through internal stress redistribution rather than free geometric expansion.

Dilation therefore introduces displacement components normal to the shear surface, expressed either as observable outward movement where confinement is low or as increased internal stresses where confinement is high. In contrast, when dilation is suppressed ($\psi_j = 0$), post-failure displacements tend to be concentrated predominantly in the shear direction, with little or no associated volumetric response.

5.2 Normal Stress Evolution and Dilatancy Resistance

Dilation directly influences the normal stress acting on a shear surface by inducing volumetric expansion during slip. When a dilating surface is free to expand—such as near a free face or excavation boundary—the dilative component is largely expressed as outward displacement, and the normal stress acting on the surface may remain low or decrease due to stress relaxation. Conversely, when dilation is restrained by surrounding confinement, volumetric expansion is inhibited and instead manifests as an increase in normal stress.

Within the ubiquitous joint formulation in FLAC3D, this behaviour is captured implicitly through the continuum response of the surrounding rock mass. Dilative plastic straining on the joint plane generates volumetric expansion, which—when constrained by the adjacent elastic material—leads to an increase in effective normal stress acting on the joint. This feedback has important mechanical implications: because shear resistance under the Mohr–Coulomb criterion depends on normal stress ($\tau = c + \sigma_n tan\,\phi$), dilation-induced increases in σ_n can transiently enhance shear resistance. This phenomenon is commonly referred to as dilatancy hardening and reflects the additional work required to continue sliding under confined conditions.

As a result, models that permit higher dilation angles tend to exhibit greater resistance to continued slip under confinement, requiring larger driving deformations to mobilize significant shear displacement. In contrast, when dilation is suppressed or absent, normal stress remains

largely unchanged during shear, allowing sliding to proceed more readily under constant confinement.

5.3 Role of Joint Normal Stiffness

In the ubiquitous joint model, the partitioning of dilative tendency between displacement and stress increase is governed not by an explicit joint stiffness, but by the stiffness and confinement of the surrounding rock mass. When the adjacent material is stiff or highly confined, even modest dilative strains can generate significant increases in normal stress, strongly limiting volumetric expansion. In such cases, dilation is accommodated primarily through stress buildup rather than geometric opening.

Conversely, in regions of low confinement or near free surfaces, the surrounding rock mass offers less resistance to dilative expansion, allowing volumetric strain to be expressed as outward displacement with relatively limited stress increase. Consequently, the apparent dilative response of ubiquitous joints is inherently scale- and confinement-dependent, reflecting the mechanical interaction between the joint plane and the surrounding continuum.

Appropriate representation of dilation therefore requires realistic modelling of both confinement and stiffness. Overestimating dilation in highly confined regions may lead to unrealistically elevated normal stresses and excessive apparent strength, while suppressing dilation entirely may underestimate deformation and strain localization near slope faces. The strain- and confinement-dependent dilation formulation adopted in this study provides a practical means of capturing this behaviour without introducing artificial stiffness parameters.

5.4 Influence on Surrounding Rock Mass Deformation

In the ubiquitous joint formulation, dilation influences not only deformation along the joint plane but also the response of the surrounding rock mass through plastic volumetric straining. As shear deformation localizes on dilating joint planes, the associated volumetric expansion produces bulking of the affected zones, which in turn imposes displacement gradients on adjacent material. These gradients induce secondary movements away from the failure surface and contribute to broader deformation patterns.

For example, dilation associated with a sub-horizontal joint set may result in upward displacement of overlying zones, whereas a purely non-dilative shear response would produce predominantly relative sliding with minimal normal displacement. In rock masses containing multiple joint sets or a pervasive ubiquitous joint fabric, the cumulative effect of such volumetric expansion can lead to global deformation responses, including floor heave or outward displacement around excavations.

While these responses are mechanically plausible, they are highly sensitive to the assumed dilation behaviour. Unrealistically high dilation angles may exaggerate volumetric expansion and displacement magnitudes, underscoring the importance of calibrating dilation parameters to representative joint conditions.

5.5 Interpretation of Numerical Displacement Results

When dilation is active in FLAC3D models employing the ubiquitous joint formulation, several characteristic features may be observed in displacement and stress outputs. These include increased normal displacements in zones undergoing shear, reduced localization of shear displacement due to energy dissipation through volumetric expansion, and elevated reaction forces or confinement pressures where dilative deformation is restrained by surrounding material or boundary conditions.

Because dilation is represented through continuum plastic straining rather than discrete joint opening, these effects arise from the interaction between the dilating joint planes and the stiffness

and confinement of the surrounding rock mass. Recognition of these signatures is essential for interpreting numerical results and for distinguishing physically meaningful deformation mechanisms from artefacts associated with simplified dilation assumptions.

6. Numerical Modelling Results

6.1 Overview of model cases

A series of numerical analyses were conducted using FLAC3D (version 9.5) to investigate the influence of joint-dilation modelling assumptions on slope deformation and stability. Although FLAC3D is a three-dimensional code, the models were configured to represent plane-strain conditions by discretizing the domain with a single zone in the out-of-plane direction. This approach enables use of the ubiquitous joint formulation while maintaining a strictly two-dimensional mechanical response appropriate for the slope geometry considered.

The primary analyses focus on an open-pit slope with an overall inclination of 49°, modelled using the ubiquitous joint formulation to represent a dominant structural fabric controlling deformation and failure. Three dilation strategies were examined:

I. Constant non-zero dilation (ψ_j = 20°), in which a uniform joint dilation angle is assigned throughout the model, independent of stress level or deformation history.
II. Constant zero dilation (ψ_j = 0°), in which dilatancy is fully suppressed to provide a lower-bound kinematic reference.
III. Strain- and confinement-dependent dilation, in which the joint dilation angle evolves as a function of accumulated plastic shear strain and effective normal stress, following the formulation described earlier.

All other model inputs—including geometry, material properties, boundary conditions, and loading—were held constant between the 49° cases to isolate the mechanical influence of the dilation formulation. The slope geometry and model configuration are illustrated in Figure 4. In addition, a steeper 60° slope was analysed to demonstrate the evolution of joint-scale constitutive response under more critical geometry; results from this case are presented separately in Figure 7.

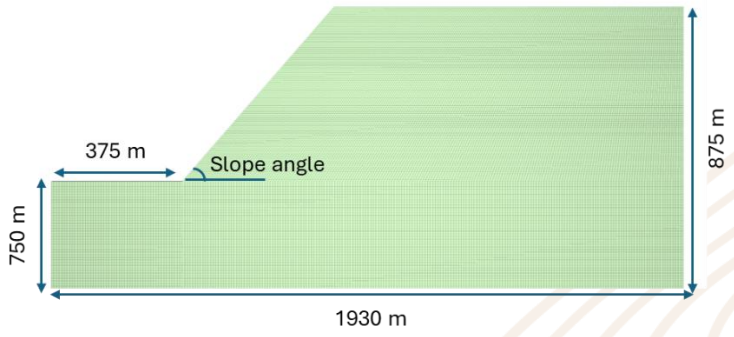


Figure 4. Model configuration for slope geometry.

6.2 Modelling methodology and model inputs

The numerical model represents the slope as a single rock mass unit without explicit inclusion of major geological structures such as faults. Structural anisotropy is captured through the ubiquitous joint formulation, with material properties for the rock matrix and joints summarized in Tables 3–5.

The intact rock matrix is modelled using the Hoek–Brown constitutive criterion with strain-softening behaviour. To isolate the mechanical influence of joint-controlled deformation and dilation, the matrix strength was deliberately set sufficiently high to prevent matrix yielding under the simulated stress conditions. As a result, plastic deformation is governed exclusively by the ubiquitous joint mechanism.

Slope stability is assessed using the Shear Strength Reduction (SSR) method, with the Strength Reduction Factor (SRF) used as an indicator of stability. Instability is identified when zone velocities exceed a prescribed threshold.

Vertical stresses are initialized as lithostatic, with horizontal stresses defined using a horizontal-to-vertical stress ratio of $K_0 = 1.0$. Lateral boundaries are fixed horizontally but free vertically, the model base is fixed vertically, and all displacements are reset to zero prior to excavation.

Table 3. Yielding model and deformability properties for rock matrix

Yielding Model	UCS (MPa)	Mi (-)	GSI (-)	Peak Young's Modulus (GPa)	Res. Young's Modulus (GPa)	Poisson's Ratio (-)	Critical Strain (-)
H-B with Strain-Softening	82.4	30	46	7.13	3.57	0.25	0.001

Table 4. Orientation and strength properties for ubiquitous joints

Yielding Model	Dip/DipDir (°)	Peak/Res. Joint Cohesion (KPa)	Peak/Res. Joint Friction (°)	Peak/Res. Joint Tensile Strength (KPa)	Critical Strain (-)
M-C with Strain-Softening	031/280	50/0	30/20	0/0	0.05

Table 5. Dilation model properties for ubiquitous joints

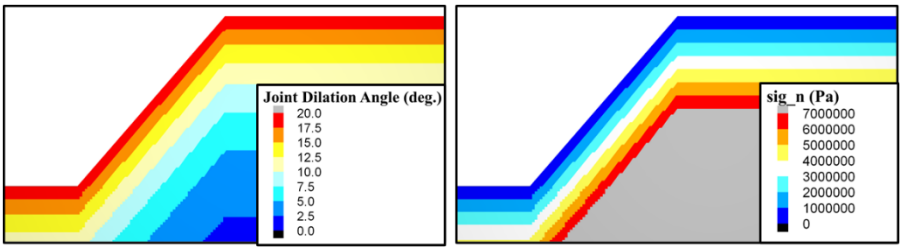
Dilation Model	Dilation Angle	$\gamma_{m,j}$ (-)	$\sigma_{n,ref,j}$ (MPa)
Uniform	20	-	-
Strain & Normal Stress Dependent	20	0.001	5

For the joint properties considered in this study, a reference normal stress of $\sigma_{n,\mathrm{ref},j} = 5$ MPa was adopted, corresponding to a 50 % reduction in dilation at moderate confinement. The characteristic strain parameter $\gamma_{m,j} = 0.001$ represents rapid post-peak degradation of joint dilation over a small amount of accumulated plastic shear strain, consistent with brittle asperity damage observed in laboratory direct shear tests and the thin shear bands typically inferred in large-scale slope models.

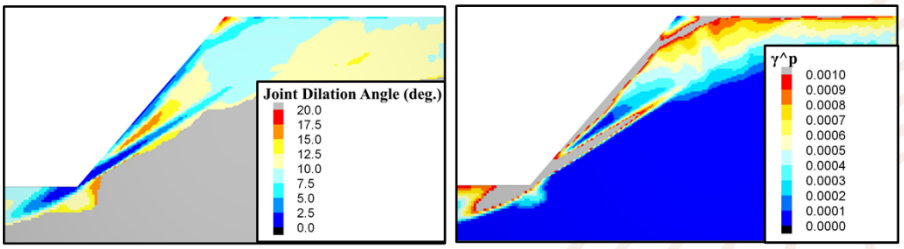
6.3 Modelling results

The numerical modelling results are summarized in Figures 5–7 and highlight the influence of joint-dilation assumptions on joint-controlled deformation and stability response. Figures 5 and 6 present results for the 49° slope, comparing the constant non-zero dilation assumption with the strain- and confinement-dependent dilation formulation under identical model geometry and inputs. Figure 5 illustrates the internal state variables governing dilation mobilization in the variable dilation model, while Figure 6 shows the resulting displacement, velocity, and strength reduction factor (SRF) distributions relative to the constant dilation assumption. In addition, a constant zero-dilation (ψ_j = 0°) case is included as a lower-bound reference to aid interpretation of the kinematic response when dilatancy is fully suppressed. Figure 7 presents results for a steeper 60° slope and is included to illustrate the evolution of joint-scale constitutive variables with cycling under more critical slope geometry.

Figure 5 shows the evolution of joint response prior to cycling and after reaching quasi-equilibrium. Before cycling, relatively high mobilized joint dilation angles are observed along the joint plane, particularly in shallow regions where effective normal stress is low. As cycling progresses and the model reaches quasi-equilibrium, accumulated joint plastic shear strain develops along a narrow band coincident with the ubiquitous joint orientation. With increasing shear strain and confinement, the mobilized dilation angle is progressively reduced, approaching near-zero values in deeper portions of the slope where normal stresses are highest. This evolution confirms that the proposed formulation behaves as intended: dilation is initially mobilized where mechanically plausible, then degraded with shear history and suppressed under increasing confinement. Importantly, plastic shear strain remains strongly localized along the joint plane throughout cycling, indicating that shear localization is governed primarily by the structural fabric rather than by the dilation formulation itself.



(a) Prior to cycling



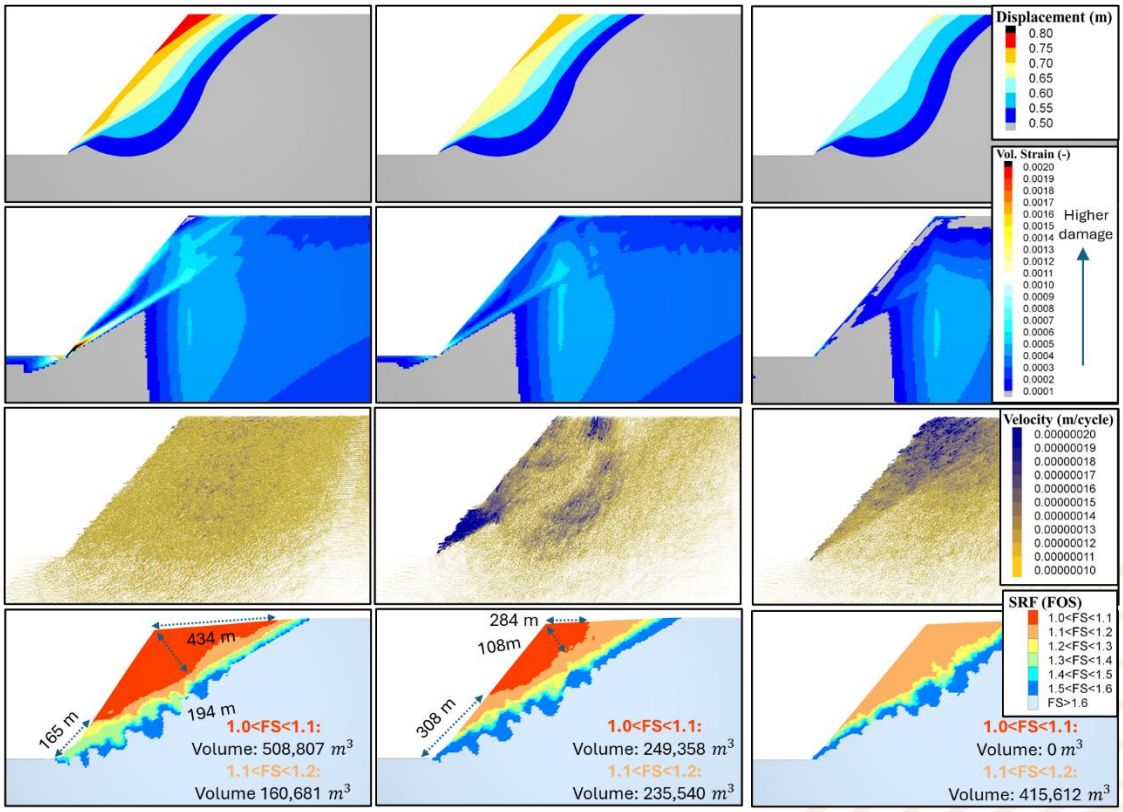
(b) After reaching quasi-equilibrium

Figure 5. FLAC3D results for the strain- and confinement-dependent dilation model for the 49° slope showing the evolution of joint response: (a) prior to cycling and (b) after reaching quasi-equilibrium. Contours illustrate the mobilized joint dilation angle ψ_j (left), effective normal stress acting on the joint plane $\sigma_{n,j}$ (top right), and accumulated joint plastic shear strain γ_j^{pl} (bottom right).

The consequences of this state-dependent dilation behaviour are evident in the deformation and stability results shown in Figure 6. Under the constant non-zero dilation model, displacement

magnitude contours form a smooth, deep-seated deformation bulb extending well into the slope interior. Although joint plastic shear strain is concentrated along a narrow zone, the constant dilation assumption allows volumetric expansion to remain active even under high confinement. This results in widespread deformation away from the shear zone and a large region of marginal stability behind the slope face, reflected by extensive areas with 1.0 < FOS < 1.1.

In contrast, the strain- and confinement-dependent dilation model produces a more confined deformation pattern. While plastic shear strain localizes along the same joint-controlled zone as in the constant dilation case, displacement magnitudes and deformation extent away from this zone are substantially reduced. Displacement contours are tighter and more sharply curved, indicating that dilation-induced volumetric expansion is largely restricted to shallow, low-confinement regions near the slope face. At depth, where Figure 5 shows elevated normal stress and accumulated plastic shear strain after cycling, dilation is suppressed and deformation decays rapidly.



(a) Constant dilation angle model - 20° (b) Strain- & normal stress-dependent model (c) Constant dilation angle model - 0°

Figure 6. FLAC3D comparison of constant non-zero, constant zero, and strain- and confinement-dependent dilation models for the 49° slope.

This difference is reflected directly in the SRF distributions. In the constant dilation model, zones of reduced SRF form a relatively thick band extending into the slope, with a substantial volume of material in marginal stability ranges. In the strain- and confinement-dependent model, reduced-SRF zones are confined to a narrow band coincident with the joint-controlled shear zone. The volume of material within the 1.0 < FOS < 1.1 range is substantially reduced compared to the constant non-zero dilation model, ψ_j = 20°, (from approximately 509,000 m³ to 249,000 m³), and the marginally stable zone is confined to a narrower band near the slope crest rather than extending deep into the slope interior. The constant zero-dilation model (ψ_j = 0°) indicates higher

FOS (FOS > 1.1) compared to the other two models, with no zones falling within the 1.0 < FOS < 1.1 range.

A key practical implication of these results is that constant-dilation models tend to predict failure mechanisms that are deeper and more broadly distributed than those typically observed in monitored open-pit slopes — a discrepancy long recognized by practitioners. The strain- and confinement-dependent formulation, by suppressing unrealistic dilation at depth, produces shallower and more spatially confined failure mechanisms that are more consistent with typical prism and LiDAR monitoring trends reported in practice.

The velocity magnitude contours in Figure 6 provide a kinematic indicator of where deformation is actively progressing rather than a direct measure of overall slope stability. For the 49° slope, all models exhibit elevated velocities as the strength reduction factor approaches instability; however, important differences are observed in the spatial distribution of these velocities. In the constant non-zero dilation model (ψ_j = 20°), non-negligible velocities extend over a broad region of the slope, reflecting continued dilation-induced volumetric straining even under high confinement. In contrast, the strain- and confinement-dependent dilation model exhibits a more localized velocity field, with higher velocities concentrated near shallow, low-confinement regions and rapid decay away from the joint-controlled shear zone. This indicates that the advanced dilation formulation primarily limits the spatial extent of active deformation rather than suppressing shear localization or altering the underlying failure kinematics.

The inclusion of a constant zero-dilation case provides an important lower-bound reference for interpreting the velocity fields. In the ψ_j = 0° model, deformation localizes almost exclusively along the joint-controlled shear zone, with negligible displacement gradients away from this surface. This behaviour reflects unrestricted shear slip in the absence of dilatancy-induced volumetric expansion or confinement-related hardening, resulting in a lower incremental energy demand for continued shear deformation (refer to Section 5.2). While velocity magnitudes may be locally elevated along the shear band, their spatial extent remains minimal. In contrast, the constant non-zero dilation model exhibits distributed velocities over a broad region of the slope due to continued volumetric straining under confinement. The strain- and confinement-dependent formulation lies between these two end-members, permitting dilation where mechanically plausible near the slope face while progressively suppressing it at depth. As a result, it produces velocity fields that are both spatially confined and mechanically consistent with expected jointed rock mass behaviour.

Figure 7 extends the analysis to a steeper 60° slope and illustrates the evolution of joint-scale response with cycling. Dilation is mobilized only in shallow, low-confinement regions and progressively suppressed with increasing normal stress and accumulated plastic shear strain, while shear deformation remains localized along the joint-controlled failure zone.

Overall, the modelling results demonstrate that incorporating strain- and confinement-dependent dilation does not alter the fundamental kinematics of failure, which remain controlled by the ubiquitous joint orientation. Instead, the advanced formulation governs the evolution and spatial extent of dilation, limiting unrealistic bulking under high confinement and reducing deformation away from the shear zone. The resulting failure mechanism for the 49° slope is thinner, more spatially confined, and mechanically more consistent with expected jointed rock mass behaviour.

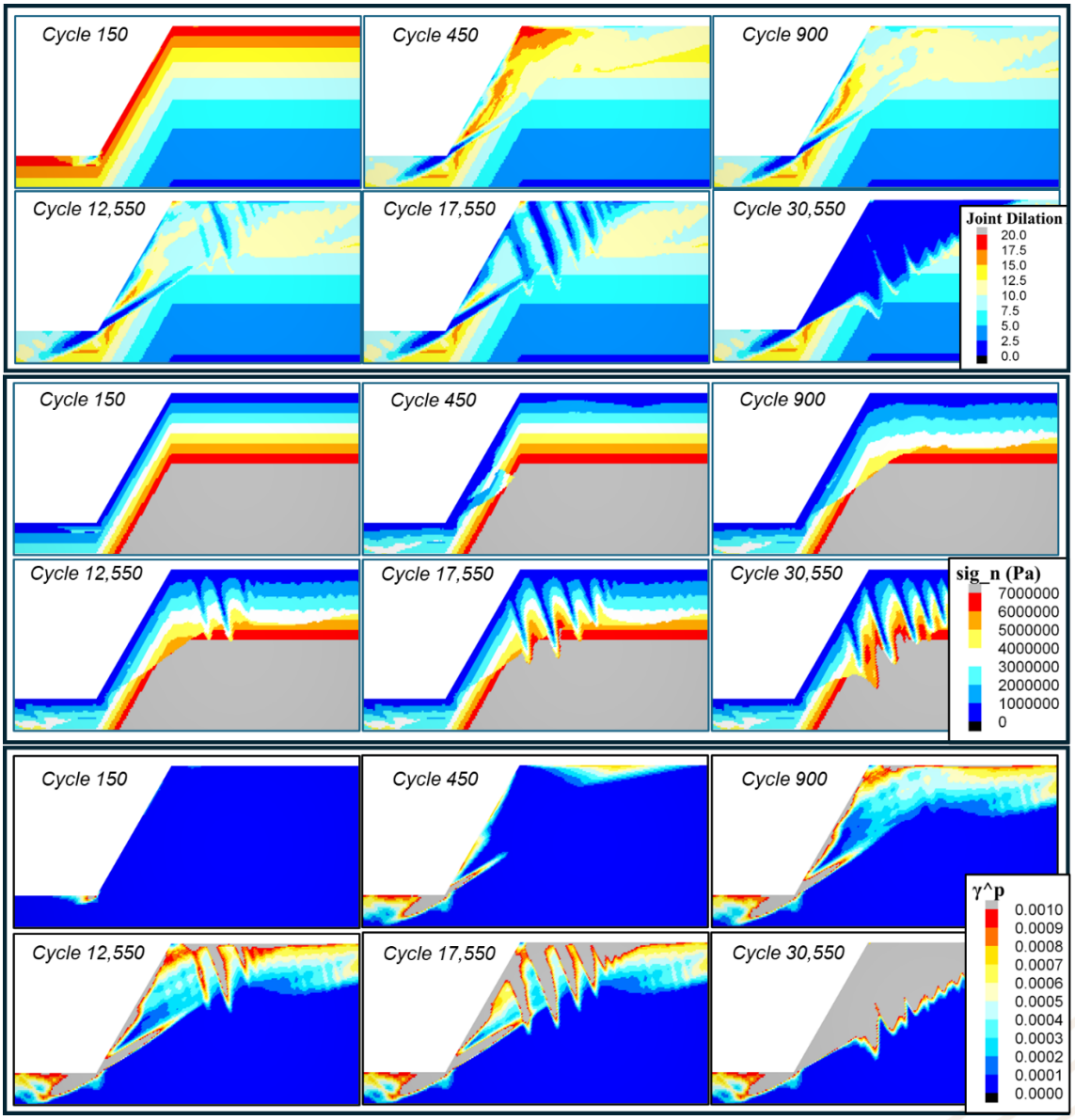


Figure 7. Evolution of joint response with cycling for a steeper 60° slope under the proposed strain- and confinement-dependent dilation formulation. Contours show the mobilized joint dilation angle ψ_j, effective normal stress acting on the joint plane $\sigma_{n,j}$, and accumulated joint plastic shear strain $\gamma^p{}_j$ at selected stages of cycling.

7. Implications for Calibration, Monitoring, and Observational Design

In open-pit mining, slope deformation is routinely monitored using surface-based instrumentation such as prism networks installed at the crest, mid-slope, and toe, as well as high-resolution LiDAR and radar systems that capture spatially continuous displacement fields. These datasets provide both the magnitude and temporal evolution of slope movements and form the primary basis for calibrating numerical models and validating assumptions related to rock mass strength, deformability, and structural behaviour. A key requirement of any calibration exercise is that the numerical model reproduces not only the onset of instability, but also the observed distribution and trend of displacements across the slope.

Simplified numerical models that adopt a constant dilation angle often struggle to reproduce these observed displacement patterns. Uniform dilation tends to generate overly stiff responses at depth and exaggerated bulking near failure surfaces, leading to displacement fields that are inconsistent

with monitored behaviour—particularly the progressive increase in displacement magnitude from toe to crest and the gradual curvature of displacement contours commonly observed in prism and LiDAR data. As a result, practitioners are often forced to compensate by unrealistically adjusting stiffness or strength parameters, thereby obscuring the physical meaning of the calibration.

In contrast, advanced dilation models that account for both strain-dependent degradation and confinement-dependent suppression of dilation provide a more realistic representation of joint-controlled deformation. By allowing dilation to mobilize near the slope face while being progressively reduced with accumulated shear strain and increasing confinement, such models are expected, based on the mechanisms captured, to more naturally reproduce displacement gradients and deformation geometries consistent with field observations — a hypothesis that follows from the modelling results presented here but that requires confirmation through calibration against site-specific monitoring records. This improved realism enables more defensible calibration against monitored displacement trends, reducing reliance on compensatory parameter adjustments. Ultimately, this enhances the reliability of observational and performance-based design approaches, where numerical models are continuously updated using monitoring data to inform risk management, trigger thresholds, and slope design decisions throughout the life of mine (LOM).

8. Conclusions

This study presents a strain- and confinement-dependent dilation formulation developed specifically for the ubiquitous joint model in FLAC3D and demonstrates its influence on predicted deformation and stability response for a joint-controlled open-pit slope. The proposed formulation allows the mobilized joint dilation angle to evolve as a function of accumulated plastic shear strain and effective normal stress, providing a physically grounded alternative to the commonly adopted constant-dilation assumption.

Numerical simulations of a 49° slope show that both constant and variable dilation models predict joint-controlled shear localization along the same structural orientation, confirming that the location of failure is governed primarily by the ubiquitous joint fabric. However, the choice of dilation formulation has a first-order effect on the magnitude and spatial extent of deformation and on the distribution of marginally stable material.

The constant dilation model permits dilation to remain active under high confinement, resulting in widespread volumetric expansion, deep-seated deformation, and large volumes of material within marginal stability ranges. In contrast, the strain- and confinement-dependent formulation suppresses dilation progressively with increasing confinement and accumulated shear strain. As a result, deformation is more tightly confined to the vicinity of the shear zone, deep-seated bulking is reduced, and the volume of marginally stable material is substantially smaller. The resulting failure mechanism is thinner, more spatially confined, and mechanically more consistent with expected jointed rock mass behaviour.

A key practical implication of these results is that constant-dilation models tend to predict failure mechanisms that are deeper and more broadly distributed than those typically observed in monitored open-pit slopes — a discrepancy long recognized by practitioners. By suppressing unrealistic dilation at depth, the strain- and confinement-dependent formulation produces shallower and more spatially confined failure mechanisms that are more consistent with typical prism and LiDAR monitoring trends reported in practice. This has direct relevance to observational and performance-based slope design, where the ability to reproduce realistic deformation patterns is essential for calibrating models against monitoring data and for establishing reliable trigger thresholds.

Importantly, the results demonstrate that the proposed formulation does not artificially force localization or alter the fundamental kinematics of failure. Instead, it improves the realism of

predicted displacement fields and stability zoning by limiting unrealistic dilation under conditions where it is mechanically implausible. This distinction is critical for slope models intended to be calibrated against monitoring data, where reproducing realistic deformation gradients is often more important than predicting ultimate failure alone. These findings are based on comparative synthetic slope models (constant, zero, and variable dilation under identical geometry) and establish the formulation's mechanical behaviour and internal consistency — but do not constitute validation against field performance.

The improved realism attributed to the formulation — displacement gradients and failure geometries more consistent with typical prism/LiDAR monitoring trends — is inferred from physical plausibility and qualitative comparison with reported patterns in the literature, not from direct comparison with an instrumented slope. Verification through back-analysis of a monitored, actively deforming pit slope is needed to confirm that the model reproduces observed displacement magnitudes, rates, and patterns at a specific site, and is identified as a priority for future work.

Overall, the strain- and confinement-dependent dilation model provides a practical and robust enhancement to the ubiquitous joint formulation widely used in industry. By embedding physically realistic dilation behaviour within a standard continuum framework, the approach improves deformation prediction, reduces reliance on compensatory parameter adjustments, and supports more defensible observational and performance-based slope design.

9. References

Barton, N. (1973). Review of a new shear strength criterion for rock joints. *Engineering Geology* 7: 287–332.

Barton, N., Bandis, S., Bakhtar, K. (1985). Strength, deformation and conductivity coupling of rock joints. *International Journal of Rock Mechanics and Mining Sciences & Geomechanics Abstracts* 22: 121–140.

Barton, N., Choubey, V. (1977). The shear strength of rock joints in theory and practice. *Rock Mechanics* 10: 1–54.

Farahmand, K., Diederichs, M.S., Baghbanan, A., Shahriar, K. (2015). Effect of fracture dilation angle on stress-dependent permeability tensor of fractured rock. In *Proceedings of the 49th US Rock Mechanics/Geomechanics Symposium*. American Rock Mechanics Association.

Farahmand, K., Rahjoo, M. (2025). Practical significance of strain-dependency and 3D-confinement-dependency of dilation mobilisation for rock slope stability evaluation. In *Proceedings of the Fourth International Slope Stability in Mining Conference (SSIM 2025)*. Australian Centre for Geomechanics.

Goodman, R.E. (1976). *Methods of Geological Engineering in Discontinuous Rocks*. West Publishing Company, St. Paul, Minnesota.

ISRM (International Society for Rock Mechanics). (1978). Suggested methods for the quantitative description of discontinuities in rock masses. *International Journal of Rock Mechanics and Mining Sciences & Geomechanics Abstracts* 15: 319–368.

Itasca Consulting Group, Inc. (2025). *FLAC3D: Fast Lagrangian Analysis of Continua in Three Dimensions, Version 9.5*. Itasca Consulting Group, Minneapolis, Minnesota.

Ladanyi, B., Archambault, G. (1969). Simulation of shear behavior of a jointed rock mass. In *Proceedings of the ARMA Symposium*. American Rock Mechanics Association.

MacDonald, N.R., Packulak, T.R., Day, J.J. (2023). A critical review of current states of practice in direct shear testing of unfilled rock fractures focused on multi-stage and boundary conditions. *Geosciences* 13: 172.

Rahjoo, M. (2019). *Directional and 3-D confinement-dependent fracturing, strength and dilation mobilization in brittle rocks*. PhD thesis, University of British Columbia, Vancouver, Canada.

Rahjoo, M., Eberhardt, E. (2021). Development of a 3-D confinement-dependent dilation model for brittle rocks; Part 2, formulation and parameterisation based on the Cartesian plastic strain increments ratios approach. *International Journal of Rock Mechanics and Mining Sciences* 148: 104773.

Sullivan, T.D. (2007). Hydromechanical coupling and pit slope movements. In Potvin, Y. (ed.), *Proceedings of Slope Stability 2007*. Australian Centre for Geomechanics, Perth, pp. 3–43.

Walton, G., Diederichs, M.S. (2015). A new model for the dilation of brittle rocks based on laboratory compression test data with separate treatment of dilatancy mobilization and decay. *Geotechnical and Geological Engineering* 33: 661–679.

Zhao, X.G., Cai, M. (2010). A mobilized dilation angle model for rocks. *International Journal of Rock Mechanics and Mining Sciences* 47: 368–384.